ADP-02/70-T510
UNITU-THEP-09/2002
hep-ph/0204178

arXiv:hep-ph/0204178v1 16 Apr 2002

Nucleon form factors from a covariant quark core: limits in their description

M. Oettel[1†*] **and R. Alkofer**[2]

[1] Special Research Centre for the Subatomic Structure of Matter,
University of Adelaide, Adelaide SA 5005, Australia
[2] Institute for Theoretical Physics, Tübingen University,
Auf der Morgenstelle 14, D-72076 Tübingen, Germany

Abstract

In treating the relativistic 3–quark problem, a dressed–quark propagator parameterization is used which is compatible with recent lattice data and pion observables. Furthermore 2–quark correlations are modeled as a series of quark loops in the scalar and axialvector channel. The resulting reduced Faddeev equations are solved for nucleon and delta. Nucleon electromagnetic form factors are calculated in a fully covariant and gauge–invariant scheme. Whereas the proton electric form factor G_E and the nucleon magnetic moments are described correctly, the neutron electric form factor and the ratio G_E/G_M for the proton appear to be quenched. The influence of vector mesons on the form factors is investigated which amounts to a 25 % modification of the electromagnetic proton radii within this framework.

PACS: 11.10.St, 12.39.Ki, 12.40.Yx, 13.40.Em, 13.40.Gp, 14.20.Dh

---

†Supported by a Feodor–Lynen fellowship of the Alexander-von-Humboldt foundation and the Australian Research Council.
*Address after April 30: MPI für Metallforschung, Heisenbergstr. 1, 70569 Stuttgart, Germany

1 Introduction

In tackling the covariant bound state problem in QCD, models based on a combined Dyson–Schwinger (DS) and Bethe–Salpeter (BS) approach have found widespread application, for recent reviews see refs. [1, 2]. This approach has been most successful in describing light pseudoscalar mesons and their electromagnetic properties. Starting from a suitable model for the gluon and the gluon–quark vertex in the infrared, and using this model consistently for the $q - \bar{q}$ scattering kernel in the meson BS equation, these mesons retain their character as both $q - \bar{q}$ bound states and Goldstone bosons. Masses [3], decay constants [4] and form factors [5] are found to be in excellent agreement with experimental data. In these studies the so–called rainbow–ladder approximation is used which consists in retaining the bare quark–gluon vertex and a gluon propagator. The latter is modeled with an enhancement at intermediate momenta which provides enough strength to generate a dynamical quark mass.

Along these lines the nucleon's bound state amplitude can be obtained by solving a relativistic Faddeev equation which needs as input the full solution for the $q - q$ scattering kernel. It is known that in the rainbow—ladder approximation this kernel exhibits diquark poles [6, 7], with scalar (0^+) diquarks ($\approx 0.7 - 0.8$ GeV) and axialvector (1^+) diquarks (≈ 0.9 GeV) having the lowest masses. Other diquark correlations have much larger masses. Although these poles might correspond to unphysical asymptotic states (and indeed disappear when going beyond rainbow–ladder [8, 9, 10]) they give us a hint that 0^+–1^+ quark–quark correlations are expected to be dominant in the nucleon. This argument receives support from recent lattice calculations [11] and also explains the u–d valence quark asymmetry observed in deep inelastic scattering [12, 13].

The full relativistic Faddeev problem is highly involved and has been solved so far only for a NJL model in lowest order where the $q - q$ interaction is pointlike and therefore separable [14]. If the $q - q$ scattering (or t) matrix is separable, the Faddeev equations reduce to a quark–diquark BS equation which can be solved exactly. Inspired by this idea, the t matrix has been modeled in such a fashion in ref. [15]. Retaining free massive quarks and 0^+–1^+ diquarks, electromagnetic, strong and weak nucleon form factors have been calculated, in good agreement with experiment (except for the magnetic form factors). It is noteworthy that especially the neutron electric form factor is positive and different from zero which is in contrast to the valence quark contributions in many non– or semi–relativistic quark models. (Due to the approximate $SU(6)$ symmetry of these models, it is consistent with zero almost by construction.) Despite the positive results of the above mentioned models, the assumptions of free massive constituent quarks and diquarks is certainly too simplistic from a QCD point of view. Another line of approach has been taken by ref. [16]. In this study, a well–constrained parametrization of the quark propagator is used which was obtained by fitting it to a number of soft and spacelike meson observables [17]. It exhibits the basic feature of DS solutions: a mass function $M(p^2)$ which is of the order of 400 MeV in the infrared and which evolves into the perturbative limit for $p^2 \to \infty$. Furthermore this parametrization has no poles thereby mimicking confinement via the absence of a Lehmann representation. Scalar diquarks and the dominant nucleon Faddeev amplitude have also been modeled with entire functions (i.e. pole–free) and the electromagnetic form factors have been calculated. The results (fitted to G_E of the proton) show also a positive neutron G_E and enhanced magnetic moments due to the dressed quark propagator which also

leads, by use of the Ward–Takahashi (WT) identity, to a dressed quark–photon vertex. A drawback of this study is the lack of manifest electromagnetic gauge invariance. In order to maintain it the calculation of currents between bound states has to proceed by gauging (i.e. minimal coupling of the photon) to an interaction kernel and sandwiching the result between bound states which are *solutions* to bound state integral equations with exactly the same kernel [18, 19].

In both studies [15, 16] the parametrization of the $q-q$ t matrix bears no relation to the quark propagator and thus to the dynamics which causes chiral symmetry breaking. There remains the possibility that the good results especially for the neutron G_E are rather a result of a clever parametrization of the $q-q$ correlations than they reflect the underlying physics. Besides the bulk of contributions to observables coming from a quark core, one would also expect corrections to these mainly coming from the pion cloud. Their non–negligeable magnitude is apparent in recent lattice extrapolations to small quark (or pion) masses [20, 21], also recent covariant studies [22, 23] confirm that the nucleon mass shift due to pions is at least -200 MeV, thereby indicating the percentage level of pionic corrections to nucleon observables.

Therefore, we will present an extension of the quark–diquark picture which, besides covariance and gauge–invariance, aims to include several constraints which are available through lattice and other QCD–phenomenological studies. Thus the number of free parameters will be confined, in fact to one, and we are in the position to explore the limits of a covariant nucleon quark core picture. We start from the main assumption to neglect three–quark irreducible interactions to arrive at solvable Faddeev equations. Evidence for this assumption is admittedly scarce, only in the limit of static quark sources lattice data [24] seem to confirm a picture where flux–tubes between each pair of the three quarks minimize the free energy of the three–quark system. Proceeding from this assumption, we employ the above mentioned efficacious quark propagator parametrization which captures the essentials of the infrared behaviour of quarks within QCD to calculate separable 0^+ and 1^+ diquark correlations by summing quark loop polarization diagrams (Sect. 2). These correlations are employed to solve the nucleon and delta Faddeev equations (Sect. 3). Parameters are fixed by the masses of nucleon and delta, leaving only one free parameter which is essentially the extension of the diquarks. Form factors are calculated in a manifestly gauge invariance preserving scheme. Here, the construction of the diquark correlations ensures that the photon properly resolves the diquark. The dependence of the form factors on the diquark width is investigated (Sect. 4). Finally, in Sect. 5, we draw our conclusions.

Throughout this paper we work in Euclidean metric ($g^{\mu\nu} = \delta^{\mu\nu}$, $\{\gamma^\mu, \gamma^\nu\} = 2\delta^{\mu\nu}$, $\gamma^{\mu\dagger} = \gamma^\mu$).

2 Diquark correlations

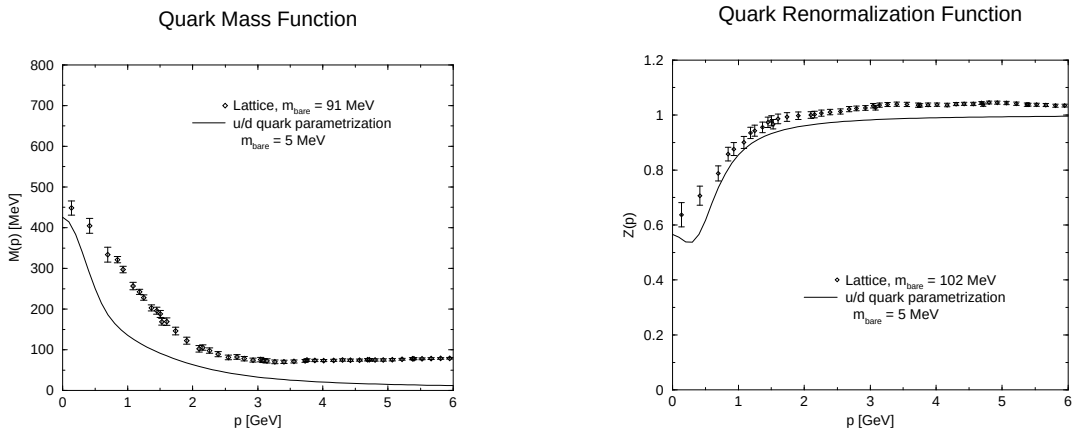

Figure 1: The quark mass function (left panel) and the renormalization function compared to lattice data.

2.1 The quark propagator

Central ingredient to all calculations is the form of the quark propagator,

$$S(p) = i\gamma \cdot p\, \sigma_V(p^2) - \sigma_S(p^2)\ , \tag{1}$$

$$= -\frac{Z(p^2)}{i\not{p} + M(p^2)} = -(i\not{p}\, A(p^2) + B(p^2))^{-1}\ . \tag{2}$$

For the scalar and vector part we use the algebraic parametrizations:

$$\bar{\sigma}_S(x) = 2\,\bar{m}\,\mathcal{F}(2(x+\bar{m}^2)) + \mathcal{F}(b_1 x)\,\mathcal{F}(b_3 x)\ [b_0 + b_2\mathcal{F}(\epsilon x)]\ , \tag{3}$$

$$\bar{\sigma}_V(x) = \frac{1}{x+\bar{m}^2}\ \left[1 - \mathcal{F}(2(x+\bar{m}^2))\right]\ , \tag{4}$$

with $\mathcal{F}(y) = (1-\mathrm{e}^{-y})/y$, $x = p^2/\lambda^2$, $\bar{m} = m/\lambda$, $\bar{\sigma}_S(x) = \lambda\,\sigma_S(p^2)$ and $\bar{\sigma}_V(x) = \lambda^2\,\sigma_V(p^2)$. The mass-scale is $\lambda = 0.566\,\mathrm{GeV}$, and the parameter values are given by

$\bar{m}$	b_0	b_1	b_2	b_3
0.00897	0.131	2.90	0.603	0.185

. (5)

In Fig. 1 we show the quark mass function $M(p^2)$ and the renormalization function $Z(p^2)$ for spacelike p in comparison with recent lattice data that have been obtained in Landau gauge [25]. Although the quark propagator fit has been performed to a number of meson observables within the DS framework [17] and *not* to lattice data, the chosen parametrization represents the qualitative behavior of both functions very well. It is still too premature to ask for quantitative agreement since lattice calculations are not feasible for current quark masses around 10 MeV yet. We note that the lattice data indicate that the slope of the decreasing mass function is somewhat less steep than in the parametrization. We will find that this slope has influence on the ratio G_E/G_M of the proton.

Both functions σ_S and σ_V are parametrized with entire functions. Thus they have no poles and reflect confinement. A major drawback, though, are the essential singularities at timelike infinity ($p^2 = -\infty$). Consequently the quark renormalization function blows up for timelike momenta, and it has been shown in ref. [26] that this has disastrous consequences if one attempts to describe production processes where timelike momenta $O(1\ \mathrm{GeV})$ are deposited onto the nucleon ($Z(-1\mathrm{GeV}^2) > 10^5$). Nevertheless, for the bound state calculations described here, the quark propagator is needed at complex momenta where always $|Z| < 1$. Due to technical obstacles we will calculate form factors only for $Q^2 < 2\ \mathrm{GeV}^2$, and for these calculations the quark propagator is sampled at momentum points where $|Z| < 1.2$. Thus for our calculations we do not expect artefacts of the parametrization to show up in the numerical results.

2.2 The $q - q$ t matrix

According to the arguments given in the Introduction, we expect scalar and axialvector $q - q$ correlations to be the most important ones within the nucleon. Thus we model a separable t matrix by

$$t(k_\alpha, k_\beta; p_\alpha, p_\beta) \equiv t(k, p, P) = \chi^5_{\alpha\beta}(k, P)\ D(P)\ \bar{\chi}^5_{\gamma\delta}(p, P)\ + \tag{6}$$

$$\chi^\mu_{\alpha\beta}(k, P)\ D^{\mu\nu}(P)\ \bar{\chi}^\nu_{\gamma\delta}(p, P)\ . \tag{7}$$

The relative momenta are defined as

$$k[p] = \frac{1}{2}(k_\alpha[p_\alpha] - k_\beta[p_\beta])\ , \tag{8}$$

and the total diquark momentum is

$$P = p_\alpha + p_\beta = k_\alpha + k_\beta\ . \tag{9}$$

We assume that the Dirac structure of the vertices χ^5 (scalar diquark) and χ^μ (axialvector diquark) is described by their leading components which non–relativistically correspond to quarks being in a relative s state:

$$\chi^5_{\alpha\beta}(p) = g_{0^+}(\gamma^5 C)_{\alpha\beta}\ \mathcal{F}(p^2/w_{0^+}), \tag{10}$$

$$\chi^\mu_{\alpha\beta}(p) = g_{1^+}(\gamma^\mu C)_{\alpha\beta}\ \mathcal{F}(p^2/w_{1^+})\ . \tag{11}$$

The scalar function $\mathcal{F}$ (defined below eq. (4)) describes the extension of the diquarks in their relative momentum variable, regulated by the widths w_{0^+} and w_{1^+}. Although the choice of this function is somewhat arbitrary, numerical results depend only on the diquark widths and not on the specific form chosen as we have checked by employing both monopole and dipole forms. The constants g_{0^+} and g_{1^+} are normalization constants yet to be determined.

Antisymmetry between the quarks dictates the color and flavor quantum numbers of the vertices χ. They are both in a color antitriplet representation. As $(\gamma_5 C)$ is antisymmetric, the scalar vertex must also be antisymmetric in flavor space, in contrast to the axialvector vertex which

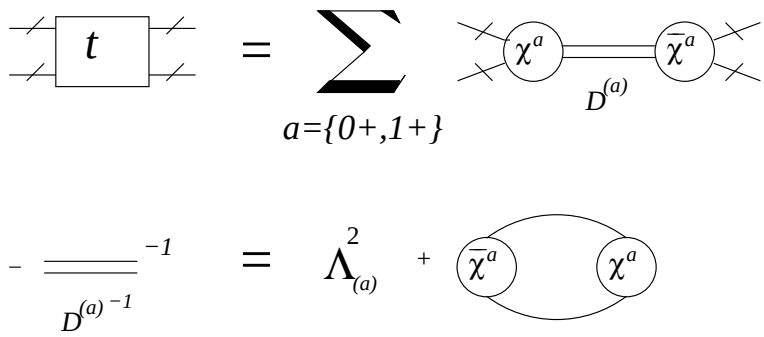

Figure 2: The separable t matrix and the definition of the diquark propagator

is symmetric in flavor space due to the symmetric matrices $(\gamma^\mu C)$. We adopt the following normalizations, restricting ourselves to the isospin subgroup:

$$(\chi^{5,C})^{AB}_{ab} = \frac{(\tau_2)_{ab}}{\sqrt{2}} \frac{\epsilon^{ABC}}{\sqrt{2}} , \tag{12}$$

$$(\chi^{\mu,C}_k)^{AB}_{ab} = \frac{(\tau_2\tau_k)_{ab}}{\sqrt{2}} \frac{\epsilon^{ABC}}{\sqrt{2}} . \tag{13}$$

Capital letters denote color indices and small letters isopin indices. The τ^k represent the usual Pauli matrices. We will suppress color and flavor indices in the following, corresponding traces will have been worked out.

We model the inverse diquark propagators D^{-1} and $(D^{\mu\nu})^{-1}$ by quark polarization diagrams as shown in Fig. 2 with an additional constant offset Λ_{0^+} for the scalar diquark and Λ_{1^+} for the axialvector diquark. This assumption describes the propagation of the quark pair being determined by an infinite series of loops as in Fig. 2. Similar expressions are obtained in the bosonized forms of the Global Color Model [27] or in the NJL model [14]. In the latter the constant Λ corresponds to the inverse strength of the four–quark interaction.

For the scalar channel the inverse propagator reads

$$D^{-1}(P^2) = -\Lambda^2_{0^+} - \Pi(P^2) , \tag{14}$$

$$\Pi(P^2) = -\int \frac{d^4q}{(2\pi)^4} \mathrm{Tr}\, \bar{\chi}^5(q^2)\, S(P/2+q)\, \chi^5(q^2)\, S^T(P/2-q) . \tag{15}$$

The polarization function $\Pi(P^2)$ has also an essential singularity at timelike infinity (as the quark propagator). Typically it evolves from $-\infty$ at $P^2 = -\infty$ monotonically to zero at $P^2 = \infty$, save for a tiny bump at around 4 GeV^2. The effect of the constant $\Lambda^2_{0^+}$ is to shift D^{-1} downwards that it acquires a zero at some $-P^2 = m^2_{0^+}$. Thus, the propagator has a pole. This is very similar to the rainbow–ladder truncation of the quark DS eq./diquark BS eq. where poles do appear in the t matrix. At the pole we demand unit residue,

$$\frac{\mathrm{d}}{\mathrm{d}P^2}\Pi(P^2)|_{P^2=-m^2_{0^+}} \stackrel{!}{=} 1 , \tag{16}$$

thus relating the hitherto unknown constant g_{0^+} to m_{0^+} or, equivalently, Λ_{0^+}.

For the inverse propagator in the axialvector channel, we employ an *ansatz* similar to the scalar channel:

$$(D^{-1})^{\mu\nu} = -\Lambda_{\rm ax}^2\, \delta^{\mu\nu} - \Pi_{\rm ax}^{\mu\nu} \ . \tag{17}$$

The polarization loop

$$\Pi_{\rm ax}^{\mu\nu}(P^2) \ = \ -\int \frac{d^4q}{(2\pi)^4} {\rm Tr}\ \bar{\chi}^\mu(q^2)\ S(P/2+q)\ \chi^\nu(q^2)\ S^T(P/2-q) \tag{18}$$

can be split into longitudinal ($P^\mu P^\nu/P^2\, \Pi_{\rm ax,L}(P^2)$) and transverse ($(\delta^{\mu\nu} - P^\mu P^\nu/P^2)\, \Pi_{\rm ax,T}(P^2)$) components. We note that $\Pi_{\rm ax,L}(0) = \Pi_{\rm ax,T}(0)$ as it should be (to have no pole in the propagator at $P^2 = 0$). Furthermore we see from the numerical results that in the region $P^2 \in [-0.7, 1.5]$ GeV $\Pi_{\rm ax,L}(P)$ is approximately constant (deviations are ≈ 1 %). Therefore we take the inverse propagator as

$$(D^{-1})^{\mu\nu}(P) = -\Lambda_{\rm ax}^2 \delta^{\mu\nu} - \Pi_{\rm ax,T}(P) \left(\delta^{\mu\nu} - \frac{P^\mu P^\nu}{P^2}\right) - \Pi_{\rm ax,T}(0)\, \frac{P^\mu P^\nu}{P^2} \ . \tag{19}$$

This is in accordance with the requirement that the longitudinal part of a spin-1 propagator not be dressed.

The behavior of the transverse polarization, $\Pi_{\rm ax,T}$, is very similar to the scalar polarization, Π, thus upon shifting by $\Lambda_{\rm ax}^2$ the propagator acquires a pole at a mass which is larger than the scalar diquark mass if $\Lambda_{0^+} \sim \Lambda_{1^+}$. At the pole a similar condition to eq. (16) holds:

$$\frac{\rm d}{{\rm d}P^2} \Pi_{\rm ax,T}(P^2)|_{P^2=-m_{1^+}^2} \stackrel{!}{=} 1 \ , \tag{20}$$

We wish to relate the constants Λ_{0^+} and Λ_{1^+} which represent inverse coupling strengths in the scalar and axialvector channels, respectively. Consider a quark vector current–current interaction where the currents are color octet and Lorentz diagonal which arises e.g. from bosonizing a Global Color Model with the gluon propagator in Feynman gauge, $\sim \delta^{\mu\nu}$. Upon a Fierz transformation into the scalar and axialvector diquark channels we find the relation [28]

$$\frac{\Lambda_{1^+}}{g_{1^+}} = 2\, \frac{\Lambda_{0^+}}{g_{0^+}} \ . \tag{21}$$

In summary, we have parametrized the $q-q$ correlations close to the rainbow–ladder truncation scheme which proved to be successful in the meson channels. Yet, scalar and axialvector diquarks are mainly characterized by an (unphysical) mass which should only be interpreted as an inverse effective correlation length than as a physical particle's mass. The composite nature of the diquarks is reflected by the propagators which are a series of quark loops. We used six parameters (diquark widths w_i, diquark normalization constants g_i and quark–quark inverse coupling strengths Λ_i, $i = \{0^+, 1^+\}$) which are reduced to three free parameters by using the relations (16,20,21). In the following, we will impose two more constraints using the masses of nucleon and delta, fixing essentially the inverse coupling strengths.

3 Faddeev equations for nucleon and delta

A full derivation of the Faddeev equations for N and Δ using separable $q-q$ t matrices can be found in ref. [29]. In the following, we will only introduce the necessary elements. For the case of separable t matrices, it is convenient to introduce baryon–quark–diquark Faddeev amplitudes. These Faddeev amplitudes have to be decomposed in Dirac and Lorentz space after their projection onto positive energy states with spin 1/2 (N) or spin 3/2 (Δ).

3.1 Nucleon

The nucleon Faddeev amplitude (or wave functions) can be described by an effective multi-spinor characterizing the scalar and axialvector correlations,

$$\Psi(p,P)u(P,s) \equiv \begin{pmatrix} \Psi^5(p,P) \\ \Psi^\mu(p,P) \end{pmatrix} u(P,s). \tag{22}$$

$u(P,s)$ is a positive-energy Dirac spinor (of spin s), p and P are the relative and total momenta of the quark-diquark pair, respectively. The vertex functions are defined by truncation of the legs,

$$\begin{pmatrix} \Phi^5 \\ \Phi^\mu \end{pmatrix} = S^{-1} \begin{pmatrix} D^{-1} & 0 \\ 0 & (D^{\mu\nu})^{-1} \end{pmatrix} \begin{pmatrix} \Psi^5 \\ \Psi^\nu \end{pmatrix}. \tag{23}$$

The coupled system of Faddeev equations for the nucleon wave and vertex functions can be written in the following compact form,

$$\int \frac{d^4k}{(2\pi)^4} G^{-1}(p,k,P) \begin{pmatrix} \Psi^5 \\ \Psi^{\mu'} \end{pmatrix} (k,P) = 0 \ , \tag{24}$$

in which $G^{-1}(p,k,P)$ is the inverse of the full quark-diquark 4-point function. It is the sum of the disconnected part and the interaction kernel.

Here, the interaction kernel results from the reduction of the Faddeev equation for separable 2-quark correlations. It describes the exchange of the quark with one of those in the diquark and thus the Faddeev equation reduces to an effective quark–diquark BS equation. Thus,

$$\begin{aligned} G^{-1}(p,k,P) \ &= \ (2\pi)^4 \ \delta^4(p-k) \ S^{-1}(p_q) \ \begin{pmatrix} D^{-1}(p_d) & 0 \\ 0 & (D^{\mu'\mu})^{-1}(p_d) \end{pmatrix} - \\ & \frac{1}{2} \begin{pmatrix} -\chi^5{}_{(p_2^2)} \ S^T{}_{(q)} \ \bar{\chi}^5{}_{(p_1^2)} & \sqrt{3} \ \chi^{\mu'}{}_{(p_2^2)} \ S^T{}_{(q)} \ \bar{\chi}^5{}_{(p_1^2)} \\ \sqrt{3} \ \chi^5{}_{(p_2^2)} \ S^T{}_{(q)} \ \bar{\chi}^\mu{}_{(p_1^2)} & \chi^{\mu'}{}_{(p_2^2)} \ S^T{}_{(q)} \ \bar{\chi}^\mu{}_{(p_1^2)} \end{pmatrix} . \end{aligned} \tag{25}$$

Herein, the flavor and color factors have been taken into account explicitly, and χ^5, χ^μ stand for the Dirac structures of the diquark-quark vertices, see eqs. (10,11). The freedom to partition the total momentum between quark and diquark introduces the parameter $\eta \in [0,1]$ with $p_q = \eta P + p$ and $p_d = (1-\eta)P - p$. The momentum of the exchanged quark is then given by

$q = -p - k + (1-2\eta)P$. The relative momenta of the quarks in the diquark vertices χ and $\bar{\chi}$ are $p_2 = p + k/2 - (1-3\eta)P/2$ and $p_1 = p/2 + k - (1-3\eta)P/2$, respectively. Invariance under (4-dimensional) translations implies that for every solution $\Psi(p, P; \eta_1)$ of the BS equation there exists a family of solutions of the form $\Psi(p + (\eta_2 - \eta_1)P, P; \eta_2)$.

Using the positive energy projector with nucleon bound-state mass M_n,

$$\Lambda^+ = \frac{1}{2}\left(1 + \frac{\not{P}}{iM_n}\right), \tag{26}$$

the wave function can be decomposed into their most general Dirac structures,

$$\Psi^5(p,P) = (S_1 + \frac{i}{M_n}\not{p} S_2)\Lambda^+, \tag{27}$$

$$\begin{aligned}\Psi^\mu(p,P) &= \frac{P^\mu}{iM_n}(A_1 + \frac{i}{M_n}\not{p} A_2)\gamma_5\Lambda^+ + \gamma^\mu(A_3 + \frac{i}{M_n}\not{p} A_4)\gamma_5\Lambda^+ \\ &+ \frac{p^\mu}{iM_n}(A_5 + \frac{i}{M_n}\not{p} A_6)\gamma_5\Lambda^+ \,.\end{aligned} \tag{28}$$

In the rest frame of the nucleon, $P = (\vec{0}, iM_n)$, the unknown scalar functions S_i and A_i are functions of $p^2 = p^\mu p^\mu$ and of the angle variable $z = \hat{P} \cdot \hat{p}$, the cosine of the (4-dimensional) azimuthal angle of p^μ. Certain linear combinations of these eight covariant components then lead to a full partial wave decomposition, see ref. [30] for more details and for examples of decomposed amplitudes assuming pointlike diquarks. Note that such a decomposition in Dirac and Lorentz space holds for the vertex function $\Phi(p, P)$ as well.

The Faddeev solutions are normalized by the canonical condition

$$\begin{aligned}M_n\Lambda^+ &\stackrel{!}{=} -\int \frac{d^4p}{(2\pi)^4}\int \frac{d^4p'}{(2\pi)^4} \\ &\bar{\Psi}(p', P_n)\left[P^\mu \frac{\partial}{\partial P^\mu} G^{-1}(p', p, P)\right]_{P=P_n} \Psi(p, P_n)\,.\end{aligned} \tag{29}$$

3.2 Delta

The effective multi-spinor for the delta baryon representing the BS wave function can be characterized as $\Psi_\Delta^{\mu\nu}(p,P)u^\nu(P)$ where $u^\nu(P)$ is a Rarita-Schwinger spinor. The momenta are defined analogously to the nucleon case. As the delta state is flavor symmetric, only the axialvector diquark contributes and, accordingly, the corresponding BS equation reads,

$$\int \frac{d^4k}{(2\pi)^4} G_\Delta^{-1}(p,k,P)\Psi_\Delta^{\mu'\nu}(k,P) = 0\,, \tag{30}$$

where the inverse quark-diquark propagator G_Δ^{-1} in the Δ-channel is given by

$$\begin{aligned}G_\Delta^{-1}(p,k,P) &= (2\pi)^4\delta^4(p-k)\; S^{-1}(p_q)\; (D^{\mu\mu'})^{-1}(p_d) + \\ &\quad \chi^{\mu'}(p_2^2)\; S^T(q)\; \bar{\chi}^\mu(p_1^2).\end{aligned} \tag{31}$$

Set		I	II	III	IV	V
w_{1^+}	[GeV^2]	0.4	0.6	0.8	1.0	1.2
w_{0^+}	[GeV^2]	0.21	0.27	0.32	0.36	0.39
m_{1^+}	[GeV]	0.92	0.91	0.89	0.88	0.87
m_{0^+}	[GeV]	0.75	0.77	0.80	0.84	0.86

Table 1: Five parameter sets which describe the physical masses of N, M_n =940MeV, and Δ, m_Δ =1230MeV.

The general decomposition of the corresponding vertex function $\Phi_\Delta^{\mu\nu}$, obtained as in eq. (23) by truncating the quark and diquark legs of the BS wave function $\Psi_\Delta^{\mu\nu}$, reads

$$\begin{aligned}\Phi_\Delta^{\mu\nu}(p,P) &= (D_1 + \frac{i}{M_\Delta}\not{p} D_2)\ \Lambda^{\mu\nu} + \frac{P^\mu}{iM_\Delta}(E_1 + \frac{i}{M_\Delta}\not{p} E_2)\frac{p_{\rm T}^\lambda}{iM_\Delta}\Lambda^{\lambda\nu} + \\ &\gamma^\mu(E_3 + \frac{i}{M_\Delta}\not{p} E_4)\frac{p_{\rm T}^\lambda}{iM_\Delta}\Lambda^{\lambda\nu} + \frac{p^\mu}{iM_\Delta}(E_5 + \frac{i}{M_\Delta}\not{p} E_6)\frac{p_{\rm T}^\lambda}{iM_\Delta}\Lambda^{\lambda\nu}\ .\end{aligned} \tag{32}$$

Here, $\Lambda^{\mu\nu}$ is the Rarita-Schwinger projector,

$$\Lambda^{\mu\nu} = \Lambda^+\left(\delta^{\mu\nu} - \frac{1}{3}\gamma^\mu\gamma^\nu + \frac{2}{3}\frac{P^\mu P^\nu}{M_\Delta^2} - \frac{i}{3}\frac{P^\mu\gamma^\nu - P^\nu\gamma^\mu}{M_\Delta}\right) \tag{33}$$

which obeys the constraints

$$P^\mu\Lambda^{\mu\nu} = \gamma^\mu\Lambda^{\mu\nu} = 0. \tag{34}$$

Therefore, the only non-zero components arise from the contraction with the transverse relative momentum $p_{\rm T}^\mu = p^\mu - \hat{P}^\mu(p\cdot\hat{P})$. The invariant functions D_i and E_i in eq. (32) again depend on p^2 and $\hat{p}\cdot\hat{P}$. The partial wave decomposition in the rest frame is given in ref. [30].

3.3 Numerical solutions

The Faddeev equations for N and Δ are solved in the baryon rest frame by expanding the unknown scalar functions in terms of Chebyshev polynomials of the variable $\hat{p}\cdot\hat{P}$ [31]. Thus the equations are reduced to a system of homogeneous one–dimensional integral equations. Iterating the integral equations yields a certain eigenvalue which by readjusting the parameters of the model is tuned to one. As remarked earlier, we are left with one free parameter which is taken to be the width w_{1^+} of the axialvector diquark.

In Tab. 1 we show five parameter sets which lead to a bound nucleon and delta with the correct physical masses, $M_n = 0.94$ GeV and $M_\Delta = 1.23$ GeV. Instead of the Λ parameters the pole locations in the diquark propagators are tabulated which have a more intuitive interpretation.

We need always a broader axialvector diquark (in momentum space) to fit both nucleon and delta. The resulting diquark masses, notably the mass difference $m_{1^+} - m_{0^+}$, agrees approximately with previous rainbow–ladder results [6, 7] only for the first two sets with smaller

diquark widths. The lattice results of ref. [11] give $m_{0^+} = 0.83$ GeV and $m_{1^+} = 0.9$ GeV, within the spread of our parameter sets.

As mentioned in the introductory chapter, pions are expected to reduce the nucleon mass by at least 200 MeV [22]. The corresponding mass shift for the delta will be lower. Therefore we investigate the Faddeev equations for nucleon and delta core states of mass 1.2 and 1.4 GeV respectively and present the results in Appendix A.

4 Nucleon form factors

4.1 Electromagnetic gauge invariance

To calculate form factors, we apply the gauging formalism of ref. [18] which basically consists in coupling the photon to all elements in the kernel G^{-1} of the nucleon Faddeev equation (24). Therefore we need the photon vertices with quark, diquarks and the quark exchange kernel. Each vertex has to satisfy its WT identity.

For the quark–photon vertex $\Gamma^\mu_q = \Gamma^\mu_{q,\mathrm{BC}} + \Gamma^\mu_{q,\mathrm{T}}$ the construction of the longitudinal part, $\Gamma^\mu_{q,\mathrm{BC}}$, which is fixed by the WT identity has been long known [32]. It is given by

$$\Gamma^\mu_{q,\mathrm{BC}}(k,p) = -i\gamma^\mu \frac{A_k + A_p}{2} - i(p+k)^\mu \frac{\not{k} + \not{p}}{2} \Delta A - (p+k)^\mu \Delta B \tag{35}$$

where $\Delta X = (X_k - X_p)/(k^2 - p^2)$ and $X_k = X(k^2)$, $(X = \{A, B\})$. The remaining transverse part, $\Gamma^\mu_{q,\mathrm{T}}$ is yet undetermined. To ensure multiplicative renormalizibility at the one–loop level, an *ansatz* for this part was proprosed in ref. [33] but it modifies our results for form factors only on the level of one per cent. The transverse part might also receive dynamical contributions from the $\rho - \omega$ meson poles in the $q - \bar{q}$ vector channel [34]. In Appendix B, we derive a parametrization of such ontributions which is well–constrained by the *pion* form factor. It is given by

$$\Gamma^\mu_{q,\mathrm{T}}(k,p) = \phi^\mu \frac{m_\rho}{f_\rho} \frac{Q^2}{Q^2 + m_\rho^2} e^{-\alpha\left(1 + \frac{Q^2}{m_\rho^2}\right)} , \tag{36}$$

$$\phi^\mu = \left(i\gamma^\mu_{\mathrm{T}} - 1.69 \frac{q^\mu_{\mathrm{T}}}{\omega_\rho} \right) \frac{\mathcal{F}^2(q^2/\omega_\rho^2)}{0.139} , \tag{37}$$

$$Q = k - p , \qquad q = (k+p)/2 \qquad v^\mu_{\mathrm{T}} = v^\mu - Q^\mu v \cdot Q/Q^2 .$$

The constants appearing herein are: ρ mass and decay constant $m_\rho = 0.77$ GeV and $f_\rho = 0.215$ GeV (calculated), $\alpha = 0.652$ and $\omega_\rho^2 = 0.35$ GeV^2. The structure ϕ^μ represents a properly normalized vector meson BS amplitude (see Appendix B). In eq. (36), the combination of the exponential and the propagator–like denominator parametrizes the effects of the propagation of an off-shell, composite $\rho - \omega$. For details, see ref. [34].

The diquark–photon vertices $\Gamma^\mu_{0^+}$ and $\Gamma^\mu_{1^+}$ receive contributions from four different diagrams, depicted in Fig. 3. Besides the photon coupling to the quarks within the loop we need seagull

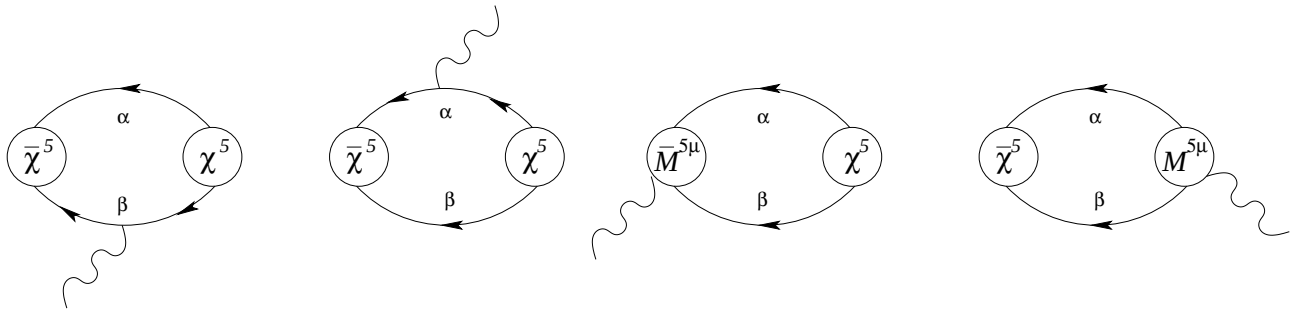

Figure 3: The photon–diquark vertex, here for the scalar diquark. For the axialvector diquark, χ^5 and $M^{5\mu}$ have to be replaced by their corresponding counterparts. Note that in actual numerical calculations the first two diagrams are equivalent if the quarks are identical.

graphs which describe the photon coupling to the vertices χ and χ^μ to recover the WT identity $(k-p)^\mu \Gamma^\mu_{0^+[1^+]} = (D^{[\mu\nu]})^{-1}(k) - (D^{[\mu\nu]})^{-1}(p)$. The functional form of these seagull vertices has been derived in ref. [19] and they read

$$\begin{aligned}(M^a)^\mu(p',Q;q_\alpha,q_\beta) &= q_\alpha \frac{(4p'-Q)^\mu}{4p'\cdot Q - Q^2}\,[\chi^a(p'-Q/2)-\chi^a(p')] + \\ &\quad q_\beta \frac{(4p'+Q)^\mu}{4p'\cdot Q + Q^2}\,[\chi^a(p'+Q/2)-\chi^a(p')]\ . \end{aligned} \tag{38}$$

The photon momentum is denoted by $Q = k - p$. The relative momentum p' between the two quarks with charges q_α and q_β has been defined in eq. (8). The conjugated vertex is obtained by replacing $\chi \to \bar{\chi}$, $Q \to -Q$ and interchanging $q_\alpha \leftrightarrow q_\beta$.

Photon–mediated transitions between scalar and axialvector diquarks are also possible. The corresponding (anomalous) vertices $\Gamma_{0^+-1^+}$ resp. $\Gamma_{1^+-0^+}$ are described by diagrams like the first two in Fig. 3. Seagulls give no contributions to these vertices.

The quark exchange kernel, as given in eq. (25), consists of expressions $\sim \chi^a\, S^T\, \bar{\chi}^b$ $(a,b = \{5,\nu\})$. Complete gauging leads to a diagram where the photon couples to the exchange quark and two diagrams where the photon couples to the vertices χ^a and $\bar{\chi}^b$. The latter couplings are described by the vertex as given in eq. (38). The proof that the gauged quark exchange kernel obeys its WT identity can be found in ref. [29].

In summary, to obtain the complete nucleon current matrix element, we have to calculate the diagrams shown in Fig. 4. We remark in passing that the normalization condition for the nucleon Faddeev amplitudes, eq. (29), is only compatible with the correct nucleon charges, i.e. $G_E(0) = 1$ (proton) and $G_E(0) = 0$ (neutron), if *all* diagrams of Fig. 4 are taken into account.

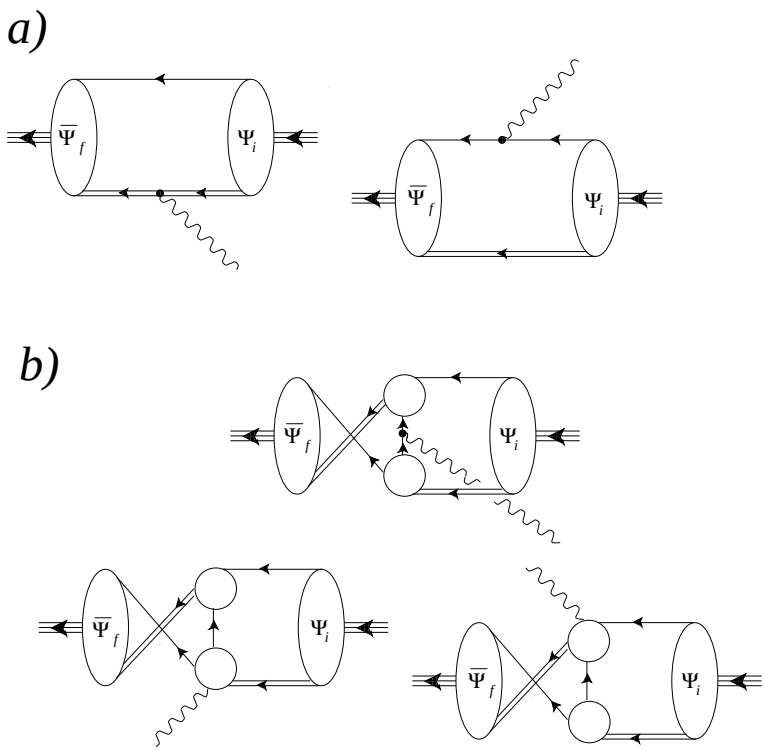

Figure 4: Nucleon current matrix elements: (a) Impulse approximation diagrams. The photon–diquark vertex consists of the elements given in Fig. 3. (b) Exchange kernel diagrams.

4.2 Numerical calculations

We extract the Sachs electromagnetic form factors from the current matrix elements by the following traces:

$$G_E(Q^2) = \frac{M_n}{2P^2} \, \mathrm{Tr} \, \langle P_f | \, J^\mu \, | P_i \rangle P^\mu \, , \tag{39}$$

$$G_M(Q^2) = \frac{iM_n^2}{Q^2} \, \mathrm{Tr} \, \langle P_f | \, J^\mu \, | P_i \rangle (\gamma^\mu)_{\mathrm{T}} \, , \qquad \left((\gamma^\mu)_{\mathrm{T}} = \gamma^\mu - \hat{P}^\mu \hat{\not{P}} \right) \, . \tag{40}$$

Here, $P = (P_i + P_f)/2$, and the initial and final states $|P_i\rangle$ and $\langle P_f|$ are given by the numerical solutions for the matrix valued wave functions $\Psi(p, P_i)$ and $\bar{\Psi}(k, P_f)$, *cf.* eqs. (22,27,28).

Due to the complicated singularity structure of the single diagrams and due to limited computer resources we obtained fairly accurate numbers for the form factors only up to momentum transfers of $Q^2 = 2$ GeV^2. These technical obstructions do not interfere with the conclusions we will draw, though. A detailed discussion of the technicalities is deferred to Appendix C.

We have calculated the form factors for the five sets tabulated in Tab. 1. The results for the electric form factors of proton and neutron are shown in Fig. 5. The proton G_E (left panel) becomes steeper with decreasing diquark widths w_{1^+} and w_{0^+}. This is in agreement with intuition since the scalar diquark correlations give the most important contributions to this

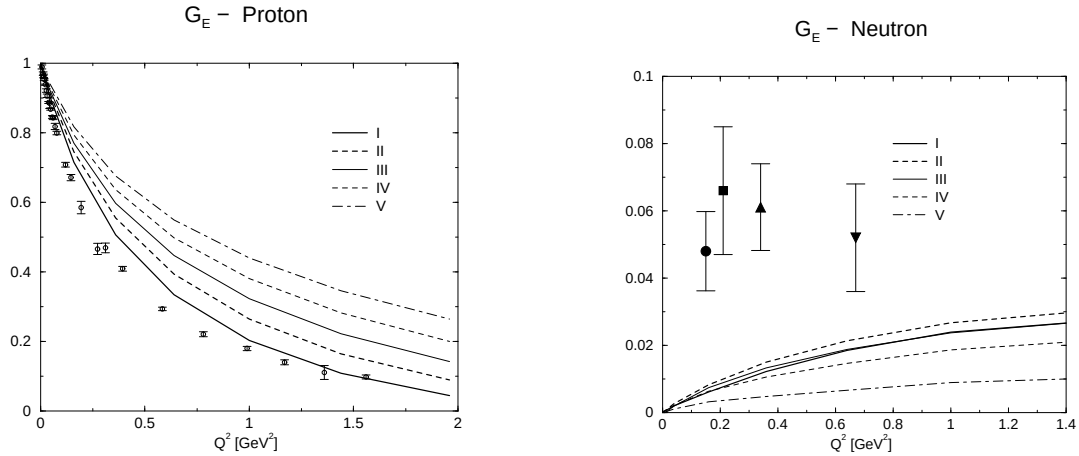

Figure 5: Depicted are the electric form factors of proton and neutron. Experimental data for the proton are taken from the analysis in ref. [35]. For the neutron, data are from ref. [36] (diamond), from ref. [37] (square), from ref. [38] (triangle up) and finally from ref. [39] (triangle down).

form factor, and with decreasing width also m_{0^+} decreases, so that these correlations become wider in the "center–of–mass" position variable as in the relative position variable. However, we also observe for Set I an interesting deviation of the form factor from the dipole shape which will be discussed below.

Let us turn to the results for G_E of the neutron (right panel in Fig. 5). All data sets predict a positive form factor which is slowly falling for larger $Q^2 > 1$ GeV^2. No data set can reproduce the experimental neutron charge radius or come close to it. This is in remarkable contrast to the results in refs. [15, 16] where rather simple parametrizations of the $q-q$ t matrix were employed. As for ref. [15], the good description of G_E was mainly a result of the cancellation between quark and diquark impulse approximation diagram. The former contribute negatively, the latter positively and by virtue of the simple approximation of the $q-q$ t matrix by free spin–0/spin–1 particles and the corresponding free photon vertices, the diquark contributions fall slower and thus render G_E positive. In this study, we have resolved the diquarks (see Fig. (3)) and the effect of diquark contributions falling more slowly is almost absent, thus the charge radius becomes very small. Only with a proper resolution of the diquarks an asymptotically correct description for the form factors is possible at all, thus we conclude that the neutron charge radius must be accounted for by other mechanisms such as a neutron dressing by pions. Nevertheless the positivity of G_E for higher momentum transfers is a result of the fully relativistic treatment.

Set		I	II	III	IV	V
μ_p	[n.m.]	3.05	2.94	2.86	2.79	2.73
μ_n	[n.m.]	−1.78	−1.65	−1.55	−1.47	−1.40

Table 2: The magnetic moments of proton (μ_p) and neutron (μ_n) for the five parameter sets given in table 1.

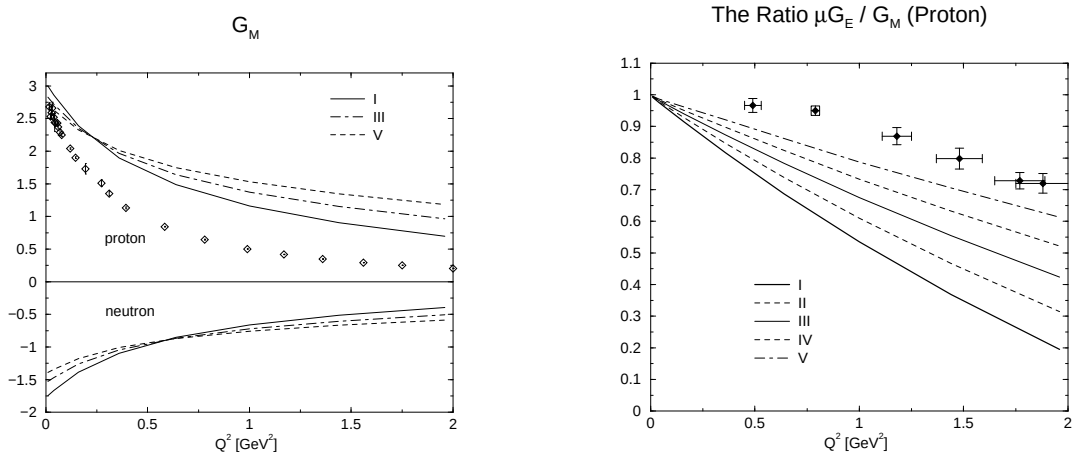

Figure 6: Magnetic form factors and G_E/G_M. Experimental data for proton's G_M are from ref. [35] and data for G_E/G_M have been reported in ref. [40].

Fig. 6, left panel, shows the nucleon magnetic form factors and Tab. 2 the corresponding magnetic moments. Also the magnetic radii become larger with decreasing diquark widths, as well as μ_p and $|\mu_n/\mu_p|$.

Our results for the ratio $\mu_p G_E/G_M$, currently under intensive experimental scrutiny, are shown in the right panel of Fig. 6. Although the results consistently put that ratio below 1, the available experimental data are underestimated considerably. Even worse, as going towards more realistic electromagnetic radii (with decreasing set number) the ratio becomes smaller and smaller. Before giving a reason for the underestimation of $\mu_p G_E/G_M$, we will examine the influence of the vector mesons in the quark–photon vertex.

Full vertex vs. Ball–Chiu vertex

Since the resonance contribution is $\sim Q^2$ near $Q^2 = 0$, it does not give any contributions to the magnetic moments, thus these are accounted for by the Ball–Chiu vertex alone. As for the pion form factor, to which the resonant vertex was fitted, it does give sizeable contribution to the charge radii. It amounts to 21–23 % in the case of $(r_p)^2_{\rm el}$ for all data sets and is therefore of the same relative size as the contribution of the resonance to the pion charge radius, see Appendix B. The neutron charge radius is usually a bit smaller, as the electric form factor is quenched a bit more when the full vertex is employed, nevertheless the differences are small and can not account for the discrepancy with the data.

In Fig. 7 we show the influence of the resonance term on proton's G_E and the ratio G_E/G_M for set II. We investigated two cases of resonance contributions, the full vertex which includes the transverse terms as in eq. 36 and a transverse vertex which includes only the leading $\gamma^\mu_{\rm T}$ term. In both cases, the vector meson amplitude is normalized and the damping constant α has been fitted to the pion form factor. For small Q^2, both resonance parametrizations lead to a G_E falling more quickly, with almost no quantitative difference. For intermediate Q^2, the subleading vector meson amplitude $\sim q_{\rm T}$ leads to a slightly enhanced G_E. This effect is visible

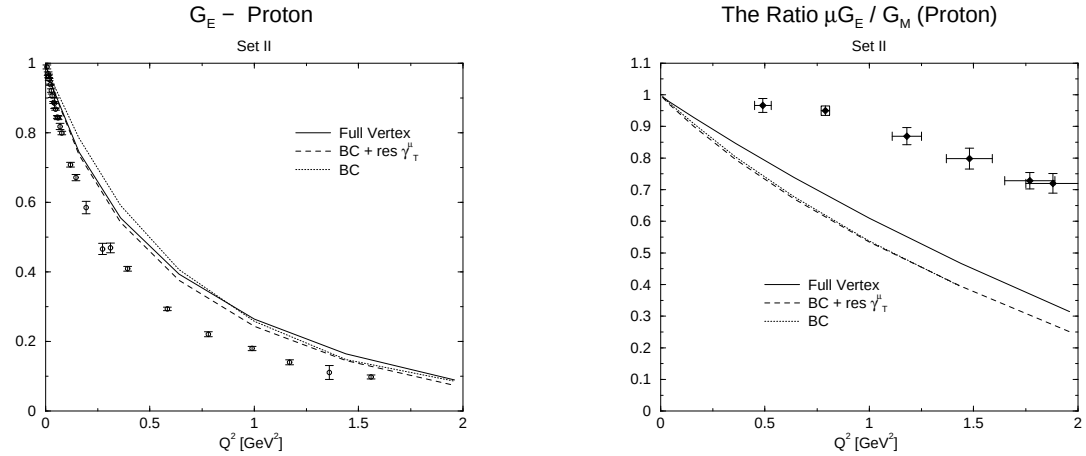

Figure 7: Comparison between results for the full vertex, the Ball–Chiu (BC) vertex plus a dominant resonance term, and the pure Ball–Chiu vertex. In the first two cases, the resonance terms have been fitted to the pion form factor.

more clearly in the ratio G_E/G_M. The subleading amplitude also quenches G_M a bit such that the ratio comes out more than 10 % larger than for the BC vertex in the intermediate Q^2 domain.

We see that the vector meson resonance has a sizeable influence on the proton charge radius (of the order 1/4), and subdominant amplitudes of the vector meson can influence G_E/G_M by 10–15 %. Nevertheless for this observable a discrepancy remains, and a reason can be found by analyzing the Ball–Chiu quark–photon vertex. This vertex always appears with quark legs attached, i.e. in the combination $\tilde{\Gamma}^\mu_q = S(k)\Gamma^\mu_{q,\mathrm{BC}}S(p)$. We rewrite $\tilde{\Gamma}^\mu_q$ in the following way:

$$\tilde{\Gamma}^\mu_q = \tilde{\Gamma}^\mu_{q,\mathrm{BC}} + \tilde{\Gamma}^\mu_{\mathrm{T}} \; . \tag{41}$$

The vertex with legs fulfills the WT identity $Q^\mu\tilde{\Gamma}^\mu_q = S(p) - S(k)$ (note that the propagator and not its inverse appears on the r.h.s.). The term $\tilde{\Gamma}^\mu_{q,\mathrm{BC}}$ is constructed via the Ball–Chiu technique to satisfy this identity:

$$\tilde{\Gamma}^\mu_{q,\mathrm{BC}}(k,p) = -i\gamma^\mu\frac{\sigma_{Vk}+\sigma_{Vp}}{2} - i(p+k)^\mu\frac{\not{k}+\not{p}}{2}\Delta\sigma_V + (p+k)^\mu\Delta\sigma_S \; . \tag{42}$$

The remainder, $\tilde{\Gamma}^\mu_{\mathrm{T}}$, is transversal, and after some Dirac algebra one finds

$$\begin{aligned}\tilde{\Gamma}^\mu_{\mathrm{T}} \;=\; & \left[Q^\mu - \gamma^\mu\not{Q} + i\Delta M(\gamma^\mu(k^2-p^2) - \not{Q}\,(k+p)^\mu)\right]\frac{i\not{p}-M_p}{p^2+M_p^2}\frac{\sigma_{Vk}}{2} - \\ & \frac{\sigma_{Vp}}{2}\frac{i\not{k}-M_k}{k^2+M_k^2}\left[Q^\mu - \not{Q}\gamma^\mu + i\Delta M(\gamma^\mu(k^2-p^2) - \not{Q}\,(k+p)^\mu)\right] \; .\end{aligned} \tag{43}$$

Due to the running mass function, the terms proportional to $\Delta M = (M(k^2)-M(p^2))/(k^2-p^2)$ are non–zero. Precisely these terms give a fairly large negative contribution to the proton's G_E, thus causing a deviation from the dipole shape. This effect is absent for G_M. Of course, a

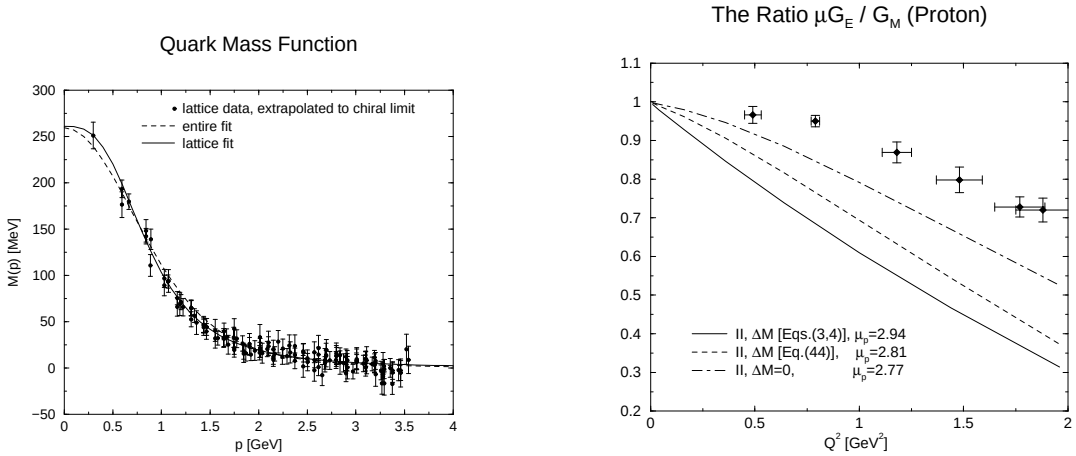

Figure 8: Left panel: lattice data from ref. [45] for the quark mass function, extrapolated to the chiral limit. Right panel: the ratio G_E/G_M for calculations with modified transverse part of the quark–photon vertex.

dynamic quark mass function of the kind depicted in Fig. 1 is phenomenologically required and thus, as in the case of the neutron electric form factor, the effect of other contributions besides the quark valence core should be sizeable for this observable. Nevertheless, some parts of the discrepancy (though not all) could be attributed to a stronger influence of the subdominant vector meson amplitudes. This amounts to a shift of the off–shell vector meson contributions between the Ball–Chiu vertex and the transverse contributions and thus between the quark propagator and the off-shell vector meson amplitudes.

To get a first estimate how a change in the quark mass function might influence the ratio G_E/G_M, we recalculated the form factors using the wave functions from parameter set II, but replaced all occurences of ΔM in the expression for $\tilde{\Gamma}^\mu_q$, eq. (43), by (a) zero (corresponding to a momentum–independent quark mass), and (b) by a fit to the most recent lattice data [45]. Since we are using wave functions calculated with the quark propagator parametrization from eqs. (3,4), this procedure is somewhat inconsistent, but may give qualitative indications to the behavior of G_E/G_M. Nevertheless, gauge invariance remains intact since the ΔM terms only appear in the transversal part of the vertex. We remarked earlier that the quenched–QCD (Landau gauge) lattice data seem to suggest a somewhat broader quark mass function than the parametrization employed here. This can be seen from Fig. 8 (left panel) where chiral limit extrapolations of the data and a fit from ref. [45] are given. Since the functional form used in the lattice fit, $M(p^2) = c\Lambda^{1+2\alpha}/(p^{2\alpha} + \Lambda^{2\alpha})$ with $\alpha = 1.52$, has a cut along the negative p^2 axis, it is not well suited for our calculations. We chose to re–fit the data to the entire function

$$M(q^2) \;=\; c_1 \left(\frac{1 - \exp(-q^2 - c_2^2)}{q^2 + c_2^2} \right)^2 , \quad [q^2 = p^2/(1\ \mathrm{GeV}^2)]. \tag{44}$$

For the choice of parameters $c_1 = 0.4$ GeV and $c_2^2 = 0.45$ our fit is also depicted in Fig. 8. We remark here that both fits, lattice and entire one, lead to a 20 % underestimation of the pion decay constant f_π (using the formula from ref. [17]), reflecting the uncertainties in lattice extrapolations and the shortcomings of the quenched approximation.

Results for the ratio G_E/G_M are plotted in Fig. 8 (right panel). The ratio is lowest for the consistent calculation. If eq. (44) is used in the vertex $\tilde{\Gamma}^\mu_q$, the curve is shifted upwards and the proton magnetic moment is somewhat smaller. Surprisingly the simple constituent quark assumption $\Delta M = 0$ delivers the best results compared to the experimental data, though employing the approximate wave functions prevents us from drawing precise quantitative conclusions. Nevertheless we see that the ratio G_E/G_M *is* sensitive to the precise form of the running quark mass. Furthermore we note that nearly the whole effect comes from the quark impulse approximation diagram (the second one in Fig. 4).

Clearly more precise QCD lattice data for the quark propagator and/or DSE/BSE studies of the three–quark and quark–photon systems are desirable.

Form factor results for nucleons with higher quark–diquark core mass are presented in Appendix A. There we find that the neutron electric form factor does not change, and that the even steeper mass function in the time–like domain deteriorates the ratio G_E/G_M even further.

5 Summary and conclusions

In a step towards the solution of the full covariant Faddeev equations for baryons, we have modeled two–quark correlations by assuming them separable and by summing quark polarization loop diagrams. In this case, the Faddeev equations reduce to a Bethe–Salpeter equation which has been solved exactly. The technique employed in calculating the two–quark correlations effectively reduced the number of model parameters to one, the diquark width.

The nucleon form factors have been calculated in a scheme which preserves the Ward–Takahashi identities for the basic two–point function, the quark propagator, for the four–point function, the quark–quark scattering kernel and finally for the quark–diquark kernel of the Faddeev equations. Consequently the current is conserved. Constrained by the pion form factor, effects from vector mesons have been included in the quark–photon vertex.

Results reveal two effects. If the proton electric and magnetic radius is to be described correctly, the ratio G_E/G_M is severely underestimated. This is a consequence of the parametrization of the dynamic mass function of quarks in accordance with results from Dyson–Schwinger and lattice studies. Furthermore the substructure of the two–quark correlations which is resolved by the photon renders the neutron form factor positive, but quite consistently for all parameter sets the corresponding charge radius cannot be described. Assuming core nucleon states with higher mass does not alter the above findings.

Certainly the precise shape of the form factors is expected to vary if the technical simplifications can be rendered obsolete, such as the separability of the two–quark correlations and the treatment of the vector meson contributions to the quark–photon vertex. Nevertheless it seems possible that the qualitative features will remain valid, i.e. the quenched neutron electric form factor for a correctly resolved $q - q$ matrix and the underestimation of G_E/G_M due to the quark–photon vertex with running mass function. As described, the vector meson contri-

butions cannot compensate this effect. The running quark mass and vector mesons are usually not considered in non– or semirelativistic quark models and urge us to a cautious interpretation of corresponding results, see e.g. ref. [41]. Thus the investigation presented in this paper point towards the necessity to incorporate non–valence quark physics into the description. Covariant studies of the effect of e.g. the pion cloud within covariant bound–state perturbation theory are clearly desirable.

Acknowledgements

We thank Craig Roberts for useful discussions in the early stages of this project.
M.O. wants to thank Tony Thomas particularly for a critical reading of the manuscript and helpful remarks. He is grateful for a shared grant by the Alexander-von-Humboldt foundation and the CSSM, Adelaide.
R.A. is grateful to the members of the CSSM, Adelaide, for their hospitality.
This work has been supported by COSY (contract no. 41376610).

A Results for core nucleon and delta states with higher mass

Pion cloud corrections will lower the mass of the nucleon by more than 200 MeV. The corresponding mass shift of the delta will be somewhat lower as the nucleon–delta mass difference is partly also a consequence of pionic dressing. For exploring effects of this shift on observables, we fix the core masses to $M_{n,\mathrm{c}} = 1.2$ GeV and $M_{\Delta,\mathrm{c}} = 1.4$ GeV. Possible parameters which lead to a solution of the Faddeev equations are given in Tab. 3. We note that less than half of the mass difference between core and physical nucleon state can be attributed to the shift in the diquark masses which are about 100 MeV larger than those in Tab. 1. If one assumed pointlike diquarks, the scalar diquark would not be changed by pionic corrections at all, but the quark substructure allows for pion dressing [42].

The proton magnetic moments are slightly reduced compared to the results for nucleons with

Set		I	II	III	IV	V
w_{1^+}	[GeV^2]	0.4	0.6	0.8	1.0	1.2
w_{0^+}	[GeV^2]	0.21	0.27	0.32	0.37	0.41
m_{1^+}	[GeV]	1.02	1.01	1.01	1.00	0.99
m_{0^+}	[GeV]	0.89	0.90	0.91	0.92	0.94

Table 3: Five parameter sets which describe core masses of nucleon and delta, $M_{n,\mathrm{c}} = 1.2$ GeV and $M_{\Delta,\mathrm{c}} = 1.4$ GeV.

		M_n [GeV]	Set	I	II	III	IV
μ_p	[n.m.]	0.94		3.05	2.94	2.86	2.79
		1.2		2.88	2.80	2.73	2.69
μ_n	[n.m.]	0.94		−1.78	−1.65	−1.55	−1.47
		1.2		−1.79	−1.69	−1.61	−1.56

Table 4: Nucleon magnetic moments, compared betweens sets with physical nucleon mass and core mass. For each pair of these sets, w_{1+} is equal and w_{0+} differs by at most 5 %.

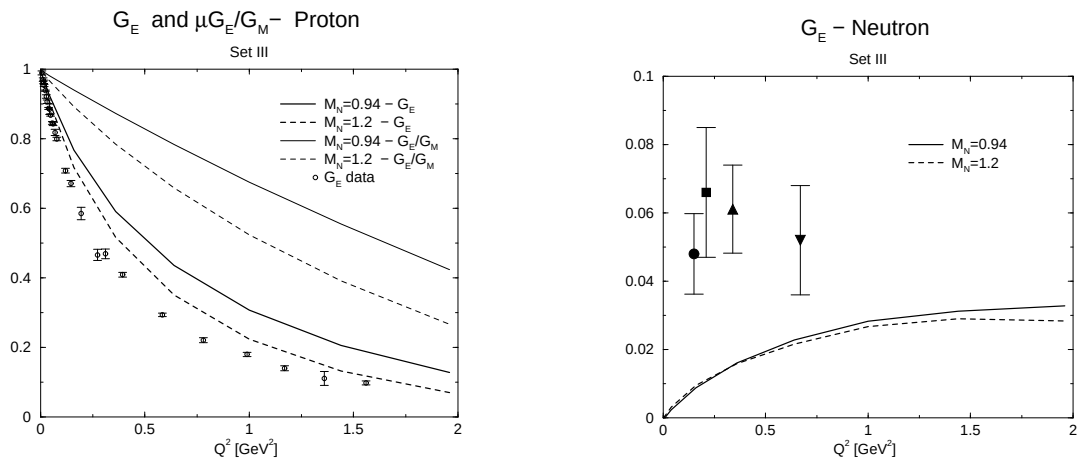

Figure 9: Form factor results compared for data sets describing nucleons with physical mass (full line) and core mass 1.2 Gev (dashed line). Left panel: proton's G_E and $\mu G_E/G_M$. Right panel: neutron's G_E.

physical mass whereas the neutron magnetic moments come out larger by a few percent, see Tab. 4. We present exemplary results for the form factors G_E and proton's G_E/G_M in Fig. 9, comparing Set III from Tabs. 1 and 3. The characteristics found here apply to the other data sets as well. The proton electric form factor becomes steeper thereby approaching the experimental curve and at the same time the ratio G_E/G_M moves even further away from the data. Since for higher core mass the quark–photon vertex tests the running mass function deeper in the timelike domain, its steeper derivative there leads to this effect. The neutron electric form factor remains unchanged.

B Resonance contribution to the quark–photon vertex

In this section we describe shortly the procedure to fix a $\rho - \omega$ resonance term in the quark–photon vertex. A somewhat longer discussion of the subject and the techniques used herein can be found in ref. [2].

The transverse part of the quark–photon vertex, $\Gamma^{\mu}_{q,\mathrm{T}}$ will certainly receive resonance contribu-

tions from the $\rho-\omega$ mesons. Assuming isospin symmetry and neglecting the decay width, the full vertex Γ_q^μ is dominated near the resonance by the term

$$\Gamma_q^\mu(k,p) = f_\rho m_\rho \frac{\phi^\mu(q;Q)}{Q^2+m_\rho^2} \tag{45}$$

$$Q = k-p \qquad\qquad q=(k+p)/2\,. \tag{46}$$

Here, $m_\rho = 0.77$ GeV and $f_\rho = 0.216$ GeV are the mass and electromagnetic decay constant of the ρ meson. The BS amplitude $\phi^\mu(q;Q)$ of the ρ meson is transversal ($Q\cdot\phi=0$) and obeys the canonical normalization condition

$$2Q^\mu = \frac{1}{3}\,3\,\mathrm{Tr}\int\frac{d^4q}{(2\pi)^4}\bar{\phi}^\mu(q;Q)\,S(-Q/2+q)\,\phi^\mu(q;Q)\frac{\partial S(Q/2+q)}{\partial q^\mu}\,, \tag{47}$$

if we assume that an interaction kernel for the corresponding BS equation is independent of Q (as e.g. a dressed gluon exchange between the quarks). The factor 1/3 comes from the sum over the three ρ polarizations, and the factor 3 is the result of the combined flavor and color trace. In color space, both ρ and ω amplitudes are the unit matrix δ_{AB}, in flavor space we have $(\tau^3)_{ab}/\sqrt{2}$ (ρ) and $(\tau^0)_{ab}/\sqrt{2}$ (ω).

Away from the resonance mass–shell the corresponding contribution to the quark–photon vertex is not fixed uniquely. The most thorough study of it is ref. [34], which calculates the (gluon–ladder) dressed quark–photon vertex for the evaluation of the pion's form factor. The findings of ref. [34] may be neatly summarized by the following points:

- $\phi^\mu(q;Q)\approx i\gamma_\mathrm{T}^\mu\,V_1(q^2)+2q_\mathrm{T}^\mu\,V_5(q^2)$ represents a good approximation to the BS solution for the ρ meson ($v_\mathrm{T}^\mu = v^\mu - Q^\mu v\cdot Q/Q^2$). It reproduces the mass and decay width within 5 %.
- The Dirac structure $i\gamma_\mathrm{T}^\mu$ accounts also for the bulk of the resonance contribution to the pion form factor, whereas terms $\sim q_\mathrm{T}^\mu$ provide corrections to these contributions on the level of 10 %. Using the ρ BS amplitude off its mass shell in the manner of eq. (45) gave a good approximation to the quark–photon vertex resonance contributions.
- The Dirac structure $(q_\mathrm{T}^\mu - \gamma_\mathrm{T}^\mu \not{q}_\mathrm{T})\not{Q}$ becomes more important for intermediate Q^2 in the pion form factor but the off shell extrapolation of the corresponding BS amplitude structure proved to be difficult. Thus we neglect this term.

We therefore adopt an off-shell parametrization of the resonance term in the quark–photon vertex,

$$\Gamma_{q,\mathrm{T}}^\mu = \phi^\mu(q)\,\frac{m_\rho}{f_\rho}\frac{Q^2}{Q^2+m_\rho^2}\,e^{-\alpha\left(1+\frac{Q^2}{m_\rho^2}\right)}\,. \tag{48}$$

Near the ρ mass shell, $Q^2=-m_\rho^2$, eq. (48) reduces to eq. (45). The exponential ensures that for high spacelike Q^2 the resonance term vanishes and the quark–photon vertex reduces to the Ball–Chiu vertex, eq. (35). The resonance term vanishes also for $Q=0$ as it should be, since at

this kinematical point the quark–photon vertex is completely fixed by the (differential) Ward identity.

We model the ρ BS amplitude close to the results of refs. [34, 43] by employing the one–parameter form

$$\phi^\mu = \left(i\gamma^\mu_{\rm T} - 1.69 \frac{q^\mu_{\rm T}}{\omega_\rho} \right) \frac{\mathcal{F}^2(q^2/\omega_\rho^2)}{N_\rho} \tag{49}$$

The normalization constant N_ρ is implicitly given by eq. (47) and the width parameter ω_ρ will be fixed by the experimental value for the decay constant, whose theoretical expression is

$$f_\rho = \frac{1}{m_\rho} \, {\rm Tr} \int \frac{d^4q}{(2\pi)^4} (-i\gamma^\mu) \, S(-Q/2+q) \, \phi^\mu(q) \, S(Q/2+q) \Big|_{Q=(\vec{0}, i m_\rho)} . \tag{50}$$

The only unknown parameter which remains in eq. (48) is the constant α which describes the damping of the off–shell resonance contribution. We fit it to the pion form factor in the range $Q^2 = [0, 1.6]$ GeV^2 where the experimental data are well described by the monopole fit [44]

$$F_\pi(Q^2) = \frac{1}{1 + \frac{Q^2}{0.529 \ {\rm GeV}^2}} . \tag{51}$$

In impulse approximation, the pion form factor is given by

$$\begin{aligned} F_\pi(Q^2) &= \frac{3}{P^2} \, {\rm Tr} \int \frac{d^4k}{(2\pi)^4} \, \bar{\phi}_\pi(k_f^2) \, S(k_1) \, \phi_\pi(k_i^2) \, S(k_+) \, \Gamma^\mu_q(k_+, k_-) \, S(k_-) \\ k_+ &= P/2 + k + Q/2 , \qquad k_f = k + Q/4 , \\ k_- &= P/2 + k - Q/2 , \qquad k_i = k - Q/4 , \\ k_1 &= -P/2 + k , \\ Q &= (0, 0, |Q|, 0) , \qquad P = (\vec{0}, i\sqrt{m_\pi^2 + Q^2/4}) . \end{aligned} \tag{52}$$

For the region of momentum transfer in consideration, the truncation of the pion's BS amplitude to the leading amplitude which is determined by chiral symmetry,

$$\phi_\pi(p^2) = \frac{B(p^2)}{N_\pi} \, \gamma_5 , \tag{53}$$

is an excellent approximation. Indeed, the quark propagator used herein has been fitted to just give $N_\pi = f_\pi = 93$ MeV, as expected physically[1].

As a result, we obtain ρ BS amplitude width of $w_\rho^2 = 0.35$ GeV^2 which in turn gives $f_\rho = 0.214$ GeV. The damping factor $\alpha = 0.652$ results in a pion form factor as shown in Fig. 10, compared to the result obtained with only the Ball–Chiu vertex. We remark that the latter yields a pion charge radius of $r_\pi^2 = 0.31$ fm^2, whereas with the resonance contribution we obtain $r_\pi^2 = 0.44$ fm^2, in acordance with the experimental value. Thus, about 30 % of the charge radius is

[1] We normalize the pion BS amplitude in color space by δ_{AB} and in flavor space by $(\tau^k)_{ab}$

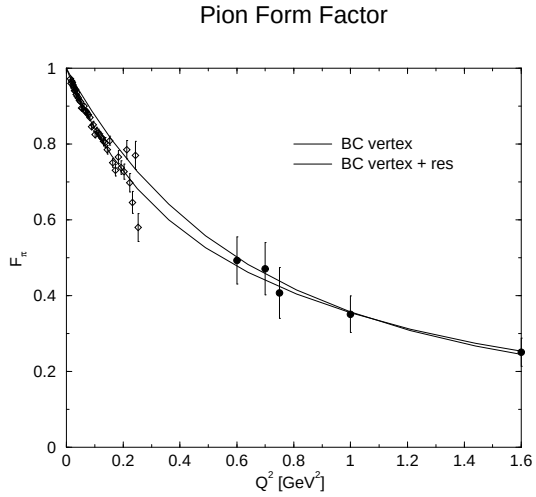

Figure 10: The pion form factor, calculated with the Ball–Chiu vertex (thin line) and the vertex including the vector meson resonance (thick line). Experimental data are from ref. [46] (diamonds) and ref. [44] (filled circles).

attributed to the vector mesons. This contribution is only half of the value obtained in ref. [34] and thus reflects the model dependence of the off–shell extrapolation: The parametrization for the quark propagator used here has a steeper $Z(p^2) = 1/A(p^2)$ than the corresponding renormalization function of the quark propagator obtained in ref. [34]. The Q^2-variation of the scalar function multiplying the dominant Dirac structure $\sim \gamma_{\rm T}^\mu$ in the quark–photon vertex is therefore already rather steep for the BC vertex used in this work and the resonance part is seen too influence the form factor only up to $Q^2 = 1$ GeV^2.

C Singularity structure of the form factor diagrams

Singularities in the diagrams are present through the quark–photon vertex Γ_q^μ, see eq. (35). It contains the scalar functions A and B which are defined by

$$A(p^2) = \frac{1}{\sigma_V(p^2)} \frac{1}{p^2 + M^2(p^2)} , \tag{54}$$

$$B(p^2) = \frac{M(p^2)}{\sigma_V(p^2)} \frac{1}{p^2 + M^2(p^2)} , \qquad (M(p^2) = \sigma_S(p^2)/\sigma_V(p^2)) . \tag{55}$$

We see that these functions have poles whenever σ_V or $p^2 + M^2$ have zeros. The poles in $1/\sigma_V$ do not matter since in the current matrix element diagrams, Γ_q^μ always appears with quark legs, $S\Gamma_q^\mu S$, and these legs cancel the pole. Such a mechanism is not present for the poles in $1/(p^2 + M^2)$. A numerical search revealed the following poles, being closest to the origin in the complex p^2 plane:

Re p^2	Im p^2
GeV^2	
-0.067	$\pm\ 0.207$
-0.167	$\pm\ 1.116$
-0.224	$\pm\ 1.360$
-0.293	$\pm\ 0.742$

We see that the pole locations appear in complex conjugate pairs. It is only the first pair of poles in the list which will have an impact on our calculations. To see that, let us consider the single form factor diagrams.

We calculate the form factors in the standard Breit frame where

$$\begin{aligned} P &= (0,0,0,i\sqrt{M^2+Q^2/4}) \\ P_i &= (0,0,-|Q|/2,i\sqrt{M^2+Q^2/4}) \\ P_f &= (0,0,+|Q|/2,i\sqrt{M^2+Q^2/4}) \end{aligned} \tag{56}$$

We start with the current matrix elements of the impulse approximation (diagrams (a) in Fig. 4). The quark diagram (where the diquark is spectator) is given by

$$\begin{aligned} \langle J_q^\mu \rangle &= \int \frac{d^4k}{(2\pi)^4} \bar{\Psi}(p_f,P_f) \begin{pmatrix} D^{-1} & 0 \\ 0 & (D^{\mu\nu})^{-1} \end{pmatrix} (k_d)\Gamma_q^\mu(k_q,p_q)\Psi(p_i,P_i) \\ p_i &= k-(1-\eta)Q/2\ , \qquad k_q = \eta P + k + Q/2\ , \\ p_f &= k+(1-\eta)Q/2\ , \qquad p_q = \eta P + k - Q/2\ , \\ k_d &= (1-\eta)P - k\ . \end{aligned} \tag{57}$$

The loop momentum k is real, but the quark momenta k_q and p_q at the vertex are not. Since their imaginary part, ηP grows with increasing Q^2, the integration domain will cross the pole locations $p^2_{\rm pole}$. The limit for Q^2 such that the integration domain will be free of these poles is

$$Q^2 < 2\,\frac{|p^2_{\rm pole}| - {\rm Re}\ p^2_{\rm pole}}{\eta^2} - 4M_n^2\ . \tag{58}$$

Beyond this limit, the integration path in the variable k_4 has to circumvent the poles or, alternatively, the sum of a principal value integral with the original path and a closed contour integral encircling the singularities must be calculated. This fact has been overlooked in ref. [16]. While this procedure has been carried out for *real* poles in ref. [19], for *complex* poles the knowledge of the wave function at *complex* relative momenta between quark and diquark is required. To obtain the wave function at these points is in principle possible, but the implementation in a current matrix element code is at present not feasible.

Choosing small momentum partitioning parameters η shifts the limit (58) to larger values. Due to the presence of the diquark pole, solutions of the Faddeev equation are restricted by $\eta > 1 - m_{0^+}/M_n$, in practice we have to restrict ourselves to $\eta = 0.32$ to have the Chebyshev expansion of the wave function converge for *both* the Faddeev solution and the calculation of the current matrix elements. This yields the limit $Q^2 < 2$ GeV^2, by virtue of eq. (58).

In the diquark diagram (with the quark being spectator), singularities occur only where the photon resolves the quark loop, i.e. in the integrals

$$\begin{aligned}
\langle J^\mu_{0^+}\rangle &= \int \frac{d^4k}{(2\pi)^4}\bar\Psi^5(p_f,P_f)S^{-1}(k_q)\Gamma^\mu_{0^+}(k_d,p_d)\Psi^5(p_i,P_i) \qquad (59)\\
p_i &= k+\eta Q/2\ , \qquad k_d=(1-\eta)P-k+Q/2\ ,\\
p_f &= k-\eta Q/2\ , \qquad p_d=(1-\eta)P-k-Q/2\ ,\\
k_q &= \eta P+k\\
\Gamma^\mu_{0^+}(k_d,p_d) &= \mathrm{Tr}\int\frac{d^4q}{(2\pi)^4}\bar\chi^5(_{q+Q/4})S(q_2)\Gamma^\mu_q(q_2,q_1)S(q_1)\chi^5(_{q-Q/4})S^T(q_3)\\
& \qquad\qquad\qquad\qquad\qquad\qquad\qquad\qquad\qquad\qquad\qquad\qquad (60)\\
q_1 &= (p_d+k_d)/4+q-Q/2\ , \qquad q_2=(p_d+k_d)/4+q+Q/2\ ,\\
q_3 &= (p_d+k_d)/4-q\ .
\end{aligned}$$

While these equations describe the contribution of the scalar diquark, similar expressions hold for the axialvector diquark and the scalar–axialvector transitions. The imaginary part of the quark momenta q_1 and q_2 which enter the quark–photon vertex is given by $(1-\eta)P/2$, therefore we can apply eq. (58) for a pole–free integration domain upon the replacement $\eta\to(1-\eta)/2$. If we want to calculate pole–free up to $Q^2=2$ GeV^2, we find $\eta>0.36$. Thus the Faddeev solutions and these diagrams have to be calculated with a *different* momentum partitioning parameter than the Faddeev solutions for the quark diagram. This is of course possible since the Faddeev solutions have been obtained fully covariantly, i.e. the full dependence of the wave function on p^2 and $p\cdot P$ has been retained (p is the relative quark–diquark momentum and P is the total nucleon momentum).

Singularities in the exchange kernel contributions (diagrams (b) in Fig. 4) are present in the diagram where the photon couples to the exchange quark. The corresponding current matrix element is given by

$$\begin{aligned}
\langle J^\mu_{ex}\rangle &= \int\frac{d^4k}{(2\pi)^4}\int\frac{d^4p}{(2\pi)^4}\bar\Psi^a(k,P_f)\chi^a(p_s)\left(S(q_1)\Gamma^\mu_q(q_1,q_2)S(q_2)\right)^T\times\\
&\qquad \bar\chi^b(k_s)\Psi^b(p,P_i) \qquad (a,b=\{5,\mu\}) \qquad (61)\\
q_1 &= -p-k+(1-2\eta)P-\frac{Q}{2}\ , \quad p_s=k+\frac{p}{2}-(1-3\eta)\frac{P}{2}-(\eta-1)\frac{Q}{4}\\
q_2 &= -p-k+(1-2\eta)P+\frac{Q}{2}\ , \quad k_s=p+\frac{k}{2}-(1-3\eta)\frac{P}{2}+(\eta-1)\frac{Q}{4}
\end{aligned}$$

Here the imaginary part of the momenta q_1 and q_2 (appearing in the quark–photon vertex) is given by $(1-2\eta)P$. Using eq. (58) again (with $\eta\to(1-2\eta)$), we find the condition $\eta>0.34$ if we want to calculate this diagram without encountering poles up to $Q^2=2$ GeV^2.

References

[1] R. Alkofer and L. von Smekal, Phys. Rept. **353** (2001) 281 [arXiv:hep-ph/0007355].

[2] C. D. Roberts and S. M. Schmidt, Prog. Part. Nucl. Phys. **45S1**, 1 (2000) [arXiv:nucl-th/0005064].

[3] R. Alkofer, P. Watson and H. Weigel, Phys. Rev. D, in print [arXiv:hep-ph/0202053]; and references therein.

[4] P. Maris and C. D. Roberts, Phys. Rev. C **56**, 3369 (1997) [arXiv:nucl-th/9708029].

[5] P. Maris and P. C. Tandy, Phys. Rev. C **62**, 055204 (2000) [arXiv:nucl-th/0005015].

[6] J. Praschifka, R. T. Cahill and C. D. Roberts, Int. J. Mod. Phys. A **4**, 4929 (1989).

[7] C. J. Burden, L. Qian, C. D. Roberts, P. C. Tandy and M. J. Thomson, Phys. Rev. C **55**, 2649 (1997) [arXiv:nucl-th/9605027].

[8] A. Bender, C. D. Roberts and L. von Smekal, Phys. Lett. B **380**, 7 (1996) [arXiv:nucl-th/9602012].

[9] G. Hellstern, R. Alkofer and H. Reinhardt, Nucl. Phys. A **625**, 697 (1997) [arXiv:hep-ph/9706551].

[10] A. Bender, W. Detmold, C. D. Roberts and A. W. Thomas, arXiv:nucl-th/0202082.

[11] I. Wetzorke and F. Karsch, arXiv:hep-lat/0008008.

[12] F. E. Close and A. W. Thomas, Phys. Lett. B **212**, 227 (1988).

[13] H. Mineo, W. Bentz, N. Ishii and K. Yazaki, arXiv:nucl-th/0201082.

[14] N. Ishii, W. Bentz and K. Yazaki, Nucl. Phys. A **587**, 617 (1995).

[15] M. Oettel, R. Alkofer and L. von Smekal, Eur. Phys. J. A **8**, 553 (2000) [arXiv:nucl-th/0006082].

[16] J. C. Bloch, C. D. Roberts, S. M. Schmidt, A. Bender and M. R. Frank, Phys. Rev. C **60**, 062201 (1999) [arXiv:nucl-th/9907120].

[17] C. J. Burden, C. D. Roberts and M. J. Thomson, Phys. Lett. B **371**, 163 (1996) [arXiv:nucl-th/9511012].

[18] A. N. Kvinikhidze and B. Blankleider, Phys. Rev. C **60**, 044003 (1999) [arXiv:nucl-th/9901001].

[19] M. Oettel, M. Pichowsky and L. von Smekal, Eur. Phys. J. A **8**, 251 (2000) [arXiv:nucl-th/9909082].

[20] R. D. Young, D. B. Leinweber, A. W. Thomas and S. V. Wright, arXiv:hep-lat/0111041.

[21] D. B. Leinweber, A. W. Thomas, K. Tsushima and S. V. Wright, Phys. Rev. D **61**, 074502 (2000) [arXiv:hep-lat/9906027].

[22] M. B. Hecht, M. Oettel, C. D. Roberts, S. M. Schmidt, P. C. Tandy and A. W. Thomas, Phys. Rev. C, in print [arXiv:nucl-th/0201084].

[23] M. Oettel and A. W. Thomas, arXiv:nucl-th/0203073.

[24] C. Alexandrou, P. De Forcrand and A. Tsapalis, Phys. Rev. D **65** (2002) 054503 [arXiv:hep-lat/0107006].

[25] J. Skullerud, D. B. Leinweber and A. G. Williams, Phys. Rev. D **64** (2001) 074508 [arXiv:hep-lat/0102013].

[26] S. Ahlig, R. Alkofer, C. Fischer, M. Oettel, H. Reinhardt and H. Weigel, Phys. Rev. D **64**, 014004 (2001) [arXiv:hep-ph/0012282].

[27] C. D. Roberts, R. T. Cahill and J. Praschifka, Annals Phys. **188**, 20 (1988).

[28] R. Alkofer and H. Reinhardt, *Chiral quark dynamics*, *Berlin, Germany: Springer (1995) 114 p. (Lecture notes in physcis).*

[29] M. Oettel, *Baryons as relativistic bound states of quark and diquark*, PhD thesis, Tübingen University 2000, http://w210.ub.uni-tuebingen.de/dbt/volltexte/2000/177 [arXiv:nucl-th/0012067].

[30] M. Oettel, G. Hellstern, R. Alkofer and H. Reinhardt, Phys. Rev. C **58**, 2459 (1998) [arXiv:nucl-th/9805054].

[31] M. Oettel, L. von Smekal and R. Alkofer, Comput. Phys. Commun. **144**, 63 (2002) [arXiv:hep-ph/0109285].

[32] J. S. Ball and T. Chiu, Phys. Rev. D **22**, 2542 (1980).

[33] D. C. Curtis and M. R. Pennington, Phys. Rev. D **42**, 4165 (1990).

[34] P. Maris and P. C. Tandy, Phys. Rev. C **61**, 045202 (2000) [arXiv:nucl-th/9910033].

[35] G. Hoehler *et al.*, Nucl. Phys. B **114**, 505 (1976) .

[36] C. Herberg *et al.*, Eur. Phys. J. A **5**, 131 (1999).

[37] I. Passchier *et al.*, Phys. Rev. Lett. **82**, 4988 (1999) [arXiv:nucl-ex/9907012].

[38] M. Ostrick *et al.*, Phys. Rev. Lett. **83**, 276 (1999).

[39] D. Rohe *et al.*, Phys. Rev. Lett. **83**, 4257 (1999).

[40] M. K. Jones *et al.* [Jefferson Lab Hall A Collaboration], Phys. Rev. Lett. **84**, 1398 (2000) [arXiv:nucl-ex/9910005].

[41] S. Boffi, M. Radici, L. Glozman, R. F. Wagenbrunn, W. Plessas and W. Klink, arXiv:hep-ph/0104223.

[42] A. N. Kvinikhidze, M. C. Birse and B. Blankleider, arXiv:hep-ph/0110060.

[43] P. Maris and P. C. Tandy, Phys. Rev. C **60**, 055214 (1999) [arXiv:nucl-th/9905056].

[44] J. Volmer *et al.* [The Jefferson Lab F(pi) Collaboration], Phys. Rev. Lett. **86**, 1713 (2001) [arXiv:nucl-ex/0010009].

[45] P. O. Bowman, U. M. Heller and A. G. Williams, arXiv:hep-lat/0203001.

[46] S. R. Amendolia *et al.* [NA7 Collaboration], Nucl. Phys. B **277**, 168 (1986).